

Positron emission tomography imaging of CD105 expression with ^{89}Zr -Df-TRC105

Hao Hong · Gregory W. Severin · Yunan Yang · Jonathan W. Engle · Yin Zhang · Todd E. Barnhart · Glenn Liu · Bryan R. Leigh · Robert J. Nickles · Weibo Cai

Received: 3 June 2011 / Accepted: 23 August 2011 / Published online: 10 September 2011
© Springer-Verlag 2011

Abstract

Purpose High tumor microvessel density correlates with a poor prognosis in multiple solid tumor types. The clinical gold standard for assessing microvessel density is CD105 immunohistochemistry on paraffin-embedded tumor specimens. The goal of this study was to develop an ^{89}Zr -based PET tracer for noninvasive imaging of CD105 expression.

Methods TRC105, a chimeric anti-CD105 monoclonal antibody, was conjugated to *p*-isothiocyanatobenzyl-desferrioxamine (Df-Bz-NCS) and labeled with ^{89}Zr . FACS analysis and microscopy studies were performed to compare the CD105 binding affinity of TRC105 and

Df-TRC105. PET imaging, biodistribution, blocking, and ex-vivo histology studies were performed on 4T1 murine breast tumor-bearing mice to evaluate the pharmacokinetics and tumor-targeting of ^{89}Zr -Df-TRC105. Another chimeric antibody, cetuximab, was used as an isotype-matched control.

Results FACS analysis of HUVECs revealed no difference in CD105 binding affinity between TRC105 and Df-TRC105, which was further validated by fluorescence microscopy. ^{89}Zr labeling was achieved with high yield and specific activity. Serial PET imaging revealed that the 4T1 tumor uptake of ^{89}Zr -Df-TRC105 was 6.1 ± 1.2 , 14.3 ± 1.2 , 12.4 ± 1.5 , 7.1 ± 0.9 , and 5.2 ± 0.3 %ID/g at 5, 24, 48, 72, and 96 h after injection, respectively ($n=4$), higher than all organs starting from 24 h after injection, which provided excellent tumor contrast. Biodistribution data as measured by gamma counting were consistent with the PET findings. Blocking experiments, control studies with ^{89}Zr -Df-cetuximab, and ex-vivo histology all confirmed the in vivo target specificity of ^{89}Zr -Df-TRC105.

Conclusion We report here the first successful PET imaging of CD105 expression with ^{89}Zr as the radiolabel. Rapid, persistent, CD105-specific uptake of ^{89}Zr -Df-TRC105 in the 4T1 tumor was observed.

Keywords CD105/endoglin · Positron emission tomography (PET) · Tumor angiogenesis · ^{89}Zr · RadioimmunoPET · TRC105

H. Hong · Y. Yang · W. Cai
Department of Radiology,
University of Wisconsin - Madison,
Madison, WI, USA

G. W. Severin · J. W. Engle · Y. Zhang · T. E. Barnhart ·
R. J. Nickles · W. Cai
Department of Medical Physics,
University of Wisconsin - Madison,
Madison, WI, USA

G. Liu
Department of Medicine,
University of Wisconsin - Madison,
Madison, WI, USA

G. Liu · W. Cai (✉)
University of Wisconsin Carbone Cancer Center,
Room 7137, 1111 Highland Ave,
Madison, WI 53705-2275, USA
e-mail: wcai@uwhealth.org

B. R. Leigh
TRACON Pharmaceuticals, Inc,
San Diego, CA, USA

Introduction

PET imaging with radiolabeled monoclonal antibodies (mAbs) has always been a dynamic area in molecular imaging [1, 2]. With a decay half-life (3.3 days) well-matched to the

circulation half-lives of antibodies (usually on the order of days), ^{89}Zr has been extensively studied over the last decade [2, 3]. The spontaneous gamma decay of ^{89}Zr , which gives rise to 909-keV photons, can be easily gated off by setting the energy window of the PET scanner. In addition, the E_{max} of 897 keV and E_{ave} of 397 keV for its positron emission can result in PET images with good spatial resolution. Recently, a feasibility study to determine the optimal dosage and timing of administration of ^{89}Zr -labeled trastuzumab (a mAb recognizing the human epidermal growth factor receptor 2) in patients with metastatic breast cancer has been reported [4]. Excellent tumor uptake in metastatic liver, lung, bone, and even brain tumor lesions was observed.

Angiogenesis is a fundamental process in the development and metastasis of solid tumors [5]. Two of the most intensively studied angiogenesis-related targets are integrin $\alpha_v\beta_3$ and vascular endothelial growth factor receptors, and several tracers targeting these two receptors are already under clinical investigation [6–8]. Another attractive target related to tumor angiogenesis is CD105 (endoglin), a 180-kDa disulfide-linked homodimeric transmembrane protein [9]. Various studies have indicated that CD105 is one of the most suitable markers for evaluating tumor angiogenesis [10, 11]. For example, high CD105 expression correlates with poor prognosis in more than ten solid tumor types [9, 10]. These findings support the role of CD105 as an optimal marker of tumor angiogenesis, underscoring its clinical potential as a prognostic, diagnostic, and therapeutic vascular target in cancer.

Noninvasive imaging of CD105 expression represents a new paradigm for the assessment of antiangiogenic therapeutic agents, as well as for the investigation of the role of CD105 during tumor angiogenesis/metastasis [12, 13]. To date, literature reports on CD105 imaging are scarce, and all are based on labeling anti-CD105 antibodies [13–22]. Another study investigated a ^{177}Lu -labeled anti-CD105 antibody for potential radioimmunotherapy applications [23]. We recently reported the first PET imaging of CD105 expression in a mouse breast cancer model with ^{64}Cu -labeled TRC105, a human/murine chimeric IgG1

mAb which binds to both human and murine CD105 [21]. When compared with other anti-CD105 antibodies, TRC105 has a very high avidity (with a K_D of 2 ng/ml) for human CD105, and is currently in a multicenter phase 1 first-in-human dose-escalation trial in the US [24]. Multiple phase 2 therapy trials are planned or underway in patients with various types of solid tumor.

The recent success of ^{89}Zr -labeled trastuzumab in patients with metastatic breast cancer clearly suggests a promising future for ^{89}Zr -based PET tracers in the clinic [4]. To date, there is no PET tracer under clinical investigation for imaging CD105 expression. Therefore, the aim of this study was to investigate ^{89}Zr -labeled TRC105 in vitro and in vivo, with the ultimate goal of applying ^{89}Zr -labeled TRC105 to clinical PET imaging of tumor angiogenesis. ^{89}Zr labeling of antibodies can be achieved through various types of chelators, primarily desferrioxamine B (Df) which can form a stable chelate with ^{89}Zr via the three hydroxamate groups [25, 26]. However, the multistep procedure used in early studies of ^{89}Zr -labeled mAbs is quite complicated and time-consuming, which makes it challenging to produce ^{89}Zr -labeled mAbs in compliance with current Good Manufacturing Practice for clinical investigations. Recently, a new bifunctional chelate was reported for ^{89}Zr labeling: *p*-isothiocyanatobenzyl-desferrioxamine B (Df-Bz-NCS) [27]. With this agent, labeling of ^{89}Zr has been significantly simplified from the initial six-step strategy into a two-step procedure, which was adopted for this study (Fig. 1).

Materials and methods

Reagents

TRC105 was provided by TRACON Pharmaceuticals (San Diego, CA). Cetuximab (a human/murine chimeric IgG1 mAb that binds to human epidermal growth factor receptor but does not cross-react with murine epidermal growth factor receptor [21]) was from Bristol-Myers Squibb

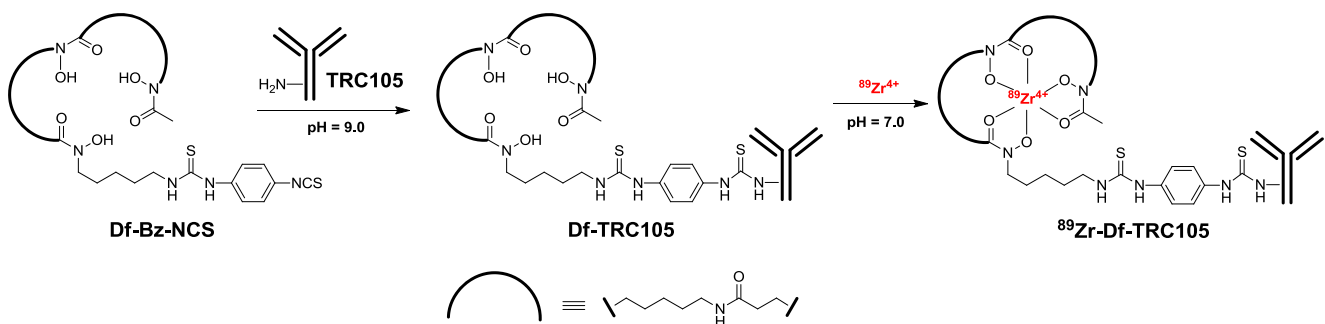


Fig. 1 The two-step procedure for ^{89}Zr -labeling of TRC105

Company (Princeton, NJ). AlexaFluor488- and Cy3-labeled secondary antibodies were purchased from Jackson ImmunoResearch Laboratories (West Grove, PA). Df-Bz-NCS and Chelex 100 resin (50–100 mesh) were purchased from Macrocylics (Dallas, TX) and Sigma-Aldrich (St. Louis, MO), respectively. Water and all buffers were of Millipore grade and pretreated with Chelex 100 resin to ensure that the aqueous solution was heavy metal-free. PD-10 desalting columns were acquired from GE Healthcare (Piscataway, NJ). All other reaction buffers and chemicals were from Thermo Fisher Scientific (Fair Lawn, NJ).

Cell lines and animal model

4T1 murine breast cancer cells, MCF-7 human breast cancer cells, and human umbilical vein endothelial cells (HUVECs) were purchased from the American Type Culture Collection (ATCC, Manassas, VA). 4T1 and MCF-7 cells were cultured in RPMI 1640 medium (Invitrogen, Carlsbad, CA) with 10% fetal bovine serum and incubated at 37°C in an atmosphere containing 5% CO₂. HUVECs were cultured in M-200 medium (Invitrogen, Carlsbad, CA) with 1×low-serum growth supplement (Cascade Biologics, Portland, OR) and incubated at 37°C in an atmosphere containing 5% CO₂. Cells were used for in vitro and in vivo experiments when they reached about 75% confluence.

All animal studies were conducted under a protocol approved by the University of Wisconsin Institutional Animal Care and Use Committee. For the 4T1 tumor model, 4- to 5-week-old female Balb/c mice were purchased from Harlan (Indianapolis, IN) and tumors were established by subcutaneously injecting 2×10^6 cells, suspended in 100 µl of a 1:1 mixture of RPMI 1640 and Matrigel (BD Biosciences, Franklin lakes, NJ), into the front flank of the mice [28]. Tumor sizes were monitored every other day and the mice were used for in vivo experiments when the diameter of tumors reached 5–8 mm (typically 1–2 weeks after inoculation).

Production of ⁸⁹Zr-oxalate

⁸⁹Zr-oxalate was produced according to the previously described procedure with minor modifications [29]. Briefly, natural yttrium foil (250 µm, 99.9%) was irradiated with a proton beam to create ⁸⁹Zr via the ⁸⁹Y(p,n)⁸⁹Zr reaction, using a 11.4-MeV CTI RDS 112 cyclotron. Irradiations typically lasted for 2 h with a current of about 5 µA, yielding 280–320 MBq of ⁸⁹Zr on the yttrium target. The foil was then dissolved in concentrated HCl (Ultrex grade, Mallinckrodt), diluted to <2 M HCl, and passed through 50–100 mg of hydroxamate resin. After washing the resin with 2 M HCl and water, the column was eluted with 1 M

oxalic acid (trace metals grade, Sigma), which typically resulted in the elution of >90% of the radioactivity in 1 ml. To calculate the specific activity of ⁸⁹Zr, the procedure above was performed on a nonirradiated yttrium foil, and the eluate was analyzed by inductively coupled plasma mass spectroscopy (ICPMS) to determine the total mass of cold Zr. Titration studies of ⁸⁹Zr-oxalate with Df mesylate (Calbiochem), analyzed by radioTLC, were also performed to validate the ICPMS results.

Df conjugation and ⁸⁹Zr labeling

Detailed procedures for Df conjugation to mAbs and subsequent ⁸⁹Zr labeling have been reported previously [26, 27]. In brief, TRC105 or cetuximab was mixed with Df-Bz-NCS at pH 9.0 at a molar ratio of 1:3. The resulting Df-TRC105 and Df-cetuximab were purified by size-exclusion chromatography. For radiolabeling, 74–148 MBq of ⁸⁹Zr-oxalate was neutralized with a 2 M Na₂CO₃ solution and added to a solution of Df-TRC105 or Df-cetuximab, using 0.05–0.35 mg of Df-mAb conjugate per 37 MBq of ⁸⁹Zr. The total reaction volume was adjusted to 2 ml with 0.5 M HEPES buffer (pH 7.1–7.3) and the reaction mixture (pH 6.8–7.2) was incubated for 1 h at room temperature (RT) with constant shaking. ⁸⁹Zr-Df-TRC105 and ⁸⁹Zr-Df-cetuximab were purified using PD-10 columns, using normal saline with 5 mg/ml of gentisic acid as the mobile phase. The radioactive fractions containing ⁸⁹Zr-Df-TRC105 or ⁸⁹Zr-Df-cetuximab were collected and passed through a 0.2-µm syringe filter for in vivo experiments.

Flow cytometry and microscopy studies

The immunoreactivities of TRC105, Df-TRC105, and Df-TRC105 after incubation in complete mouse serum at 37°C to HUVECs (high CD105 expression [17, 30]) and MCF-7 cells (CD105-negative [17]) were evaluated by fluorescence-activated cell sorting (FACS). Briefly, cells were harvested and suspended in cold PBS with 2% bovine serum albumin at a concentration of 5×10^6 cells/ml. The cells were incubated with TRC105 or Df-TRC105 (1, 5, or 15 µg/ml) for 30 min at RT, washed three times with cold PBS, and centrifuged at 1,000 rpm for 5 min. The cells were then incubated with AlexaFluor488-labeled goat anti-human IgG for 30 min at RT. Afterwards, the cells were washed and analyzed by FACS using a BD FACSCalibur four-color analysis cytometer, which is equipped with 488-nm and 633-nm lasers (Becton-Dickinson, San Jose, CA) and FlowJo analysis software (Tree Star, Ashland, OR). HUVECs were also incubated with TRC105 or Df-TRC105 (2 µg/ml) and then examined under a Nikon Eclipse Ti microscope to validate the FACS results.

Imaging and biodistribution studies

PET scans were performed using an Inveon microPET/microCT rodent model scanner (Siemens Medical Solutions USA, Inc., Malvern, PA). Each 4T1 tumor-bearing mouse was injected with 5–10 MBq of the PET tracer via a tail vein and 5-min static PET scans were performed at various time points post-injection (p.i.). The images were reconstructed using a maximum a posteriori algorithm, with no attenuation or scatter correction. For each microPET scan, three-dimensional regions of interest (ROIs) were drawn over the tumor and major organs using the vendor software (Inveon Research Workplace) on decay-corrected whole-body images. Assuming a tissue density of 1 g/ml, the ROIs were converted to MBq per gram using a conversion factor (predetermined using a 50-ml centrifuge tube filled with about 37 MBq of ^{89}Zr -oxalate as a phantom), and then divided by the total administered radioactivity to obtain an image ROI-derived percentage injected dose per gram of tissue (%ID/g). Another group of four 4T1 tumor-bearing mice was each injected with 2 mg of unlabeled TRC105 2 h earlier than ^{89}Zr -Df-TRC105 administration to evaluate the CD105 specificity of ^{89}Zr -Df-TRC105 in vivo (i.e. blocking experiment).

To anatomically localize the radioactivity signal observed on PET, a few animals were also subjected to microCT scans. Immediately after PET scanning, animals were transported to the microCT gantry, positioned, and scanned at a voxel resolution of 210 μm (scan time 7 min). Fiducial markers were used for coregistration and images were reconstructed using the vendor software (Inveon Acquisition Workshop; Siemens). The microCT and microPET datasets were loaded into the Inveon Research Workplace software and fiducial markers were coregistered for alignment of datasets.

Biodistribution studies were carried out to confirm that the quantitative tracer uptake values based on PET imaging truly represented the radioactivity distribution in tumor-bearing mice. After the last PET scan at 96 h p.i., mice were euthanized, and blood, 4T1 tumor, and major organs/tissues were collected and wet-weighed. The radioactivity in the tissue was measured using a gamma counter (Perkin Elmer) and presented as %ID/g (mean \pm SD). In addition, another group of four mice were injected with ^{89}Zr -Df-TRC105 and euthanized 24 h p.i. (when tumor uptake had reached a peak) for biodistribution studies. The 4T1 tumor, liver, spleen, and kidney (i.e. tissues with significant uptake of ^{89}Zr -Df-TRC105) were also frozen for histological analysis.

Histology

Frozen tissue slices of thickness 5 μm were fixed with cold acetone for 10 min and dried in the air for 30 min. After

rinsing with PBS and blocking with 10% donkey serum for 30 min at RT, the slices were incubated with TRC105 (2 $\mu\text{g}/\text{ml}$) for 1 h at 4°C and visualized using AlexaFluor488-labeled goat anti-human IgG. The tissue slices were also stained for endothelial marker CD31 as described previously [31, 32]. After washing with PBS, the slices were incubated with rat anti-mouse CD31 antibody (2 $\mu\text{g}/\text{ml}$) for 1 h, followed by Cy3-labeled donkey anti-rat IgG for 30 min. All images were acquired with a Nikon Eclipse Ti microscope.

Statistical analysis

Quantitative data are expressed as means \pm SD. Means were compared using Student's *t*-test. *P* values <0.05 were considered statistically significant.

Results

In vitro investigation of Df-TRC105

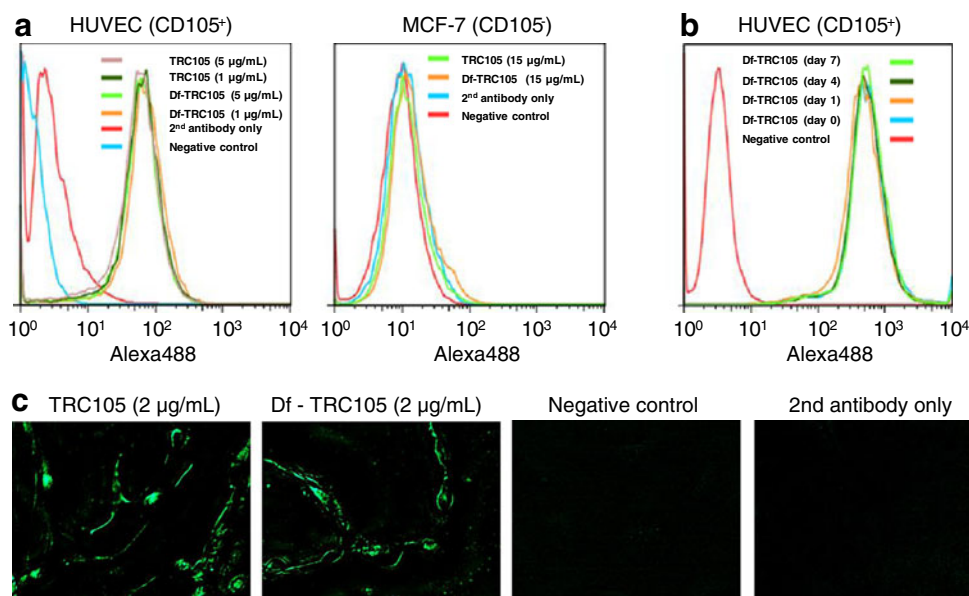
Conjugation of TRC105 to Df did not alter its CD105 binding affinity, as evidenced by both FACS analysis and fluorescence microscopy (Fig. 2). In the FACS analysis of HUVECs (which express high levels of CD105), there were no observable differences between TRC105 and Df-TRC105 at 1 $\mu\text{g}/\text{ml}$ or 5 $\mu\text{g}/\text{ml}$ (Fig. 2a). The binding to HUVECs was specific, as neither TRC105 nor Df-TRC105 bound to CD105-negative MCF-7 cells, even at the much higher concentration of 15 $\mu\text{g}/\text{ml}$ (Fig. 2a).

To evaluate its stability in serum, Df-TRC105 was incubated in complete mouse serum at 37°C for up to a week. Based on FACS analysis using HUVEC cells, no degradation in CD105 binding affinity or specificity was observed even after 7 days incubation in serum (Fig. 2b), thus confirming the superb stability of Df-TRC105. Since ^{89}Zr -Df chelate is extremely stable ($\log K > 40$), ^{89}Zr -Df-TRC105 should maintain excellent stability in vivo. In addition to FACS analysis, fluorescence microscopy was also performed on HUVECs. No significant differences between TRC105 and Df-TRC105 were observed (Fig. 2c). Taken together, these in vitro studies confirmed that Df conjugation did not alter the antigen-binding affinity or specificity of TRC105.

Specific activity measurement and ^{89}Zr -labeling

In each radiochemical separation >200 MBq of ^{89}Zr was eluted from the hydroxamate resin in the first milliliter of oxalic acid. ICPMS analysis of the eluate indicated a cold mass of 1.02 μg of Zr. Titration with Df mesylate gave consistent results, showing a reactive equivalent mass of

Fig. 2 In vitro investigation of Df-TRC105. **a** FACS analysis of TRC105 and Df-TRC105 in HUVECs (CD105-positive) and MCF-7 cells (CD105-negative) at different concentrations. **b** FACS analysis of Df-TRC105 (4 $\mu\text{g}/\text{ml}$) in HUVECs after incubation in complete mouse serum at 37°C for 1, 4, and 7 days. **c** Fluorescence microscopy images of HUVECs using either TRC105 or Df-TRC105 (2 $\mu\text{g}/\text{ml}$) as the primary antibody. Various control images are also shown



1.10 μg of Zr in the same fraction. Therefore, the specific activity of the ^{89}Zr produced for this study was 225.0 ± 23.7 MBq/ μg of Zr ($n=6$), which is comparable to the reported values for high specific activity ^{89}Zr (195–497 MBq/ μg) [33]. The specific activity of ^{89}Zr can be further improved if a longer irradiation time and/or higher beam power is used in future studies.

^{89}Zr labeling including final purification using PD-10 columns took 100 ± 10 min ($n=10$). The decay-corrected radiochemical yield was $62 \pm 15\%$, based on 0.05–0.35 mg of protein (Df-TRC105 or Df-cetuximab) per 37 MBq of ^{89}Zr , and the radiochemical purity was $>95\%$. The specific activity of both ^{89}Zr -Df-TRC105 and ^{89}Zr -Df-cetuximab was between 0.1 and 0.5 GBq/mg protein, assuming virtually complete recovery of the Df-mAb conjugates after size exclusion chromatography.

Small-animal PET imaging

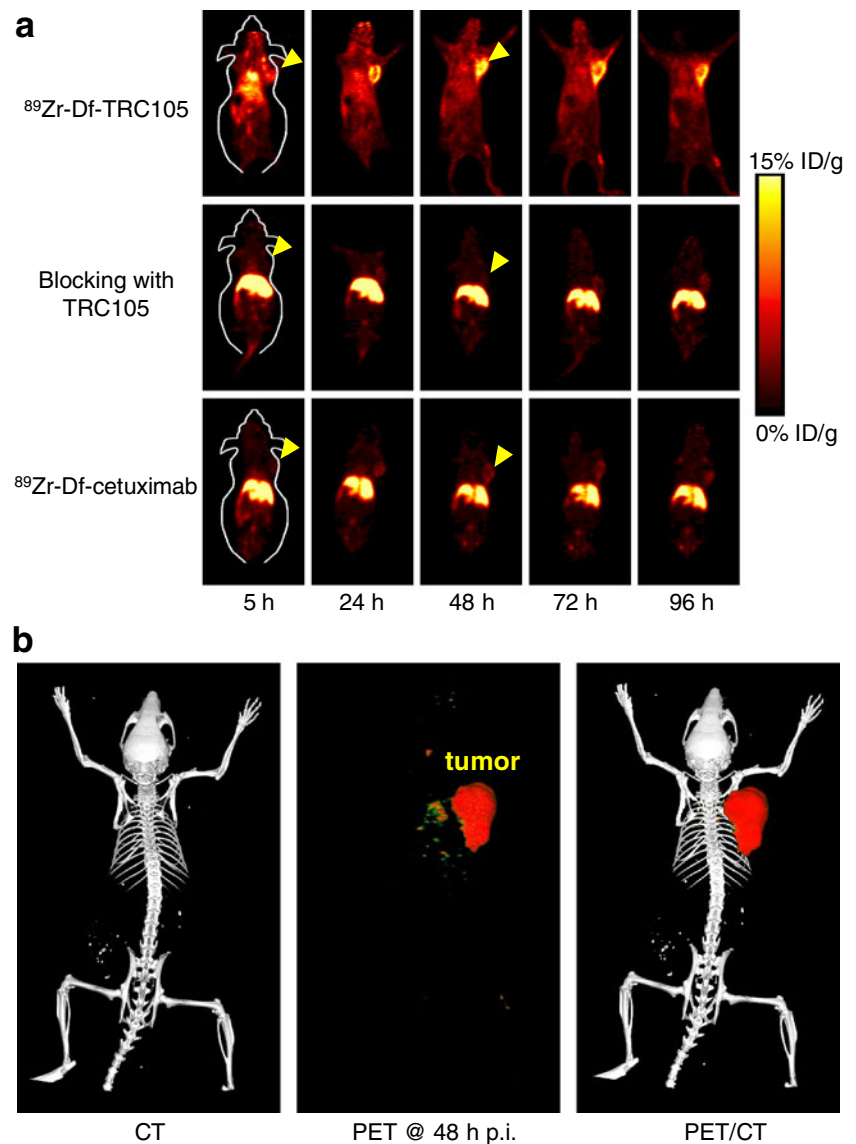
Due to the relatively long half-life of ^{89}Zr (3.3 days), which allowed investigation of ^{89}Zr -Df-TRC105 over a significantly longer time period than ^{64}Cu -labeled TRC105 [21], the time points of 5, 24, 48, 72, and 96 h were chosen for serial PET scans after intravenous tracer injection. The coronal slices that included the 4T1 tumor are shown in Fig. 3a and representative PET/CT fused images of a mouse at 48 h after injection of ^{89}Zr -Df-TRC105 are shown in Fig. 3b. The quantitative data obtained from ROI analysis are shown in Fig. 4. Due to the superb stability of the ^{89}Zr -Df conjugate, liver uptake of ^{89}Zr -Df-TRC105 was significantly lower at all time points examined than that observed for ^{64}Cu -DOTA-TRC105 (which may have a certain degree of ^{64}Cu -transchelation, thereby increasing radioactivity

accumulation in the liver) in our previous study in the same tumor model [21]. Meanwhile, blood pool activity was prominent at early time points (due to the long circulation half-life of the antibody) which gradually declined over time. The liver uptake of ^{89}Zr -Df-TRC105 was 12.4 ± 2.1 , 7.6 ± 1.5 , 5.3 ± 0.2 , 2.9 ± 0.1 , and 2.3 ± 0.1 % ID/g at 5, 24, 48, 72, and 96 h p.i. respectively, while the radioactivity in the blood was 14.7 ± 2.5 , 9.9 ± 1.9 , 6.8 ± 0.7 , 3.5 ± 0.5 , and 2.0 ± 0.4 % ID/g at 5, 24, 48, 72, and 96 h p.i., respectively ($n=4$; Fig. 4a). Tumor uptake of ^{89}Zr -Df-TRC105 was clearly visible as early as 5 h p.i. and reached a peak at around 24 h p.i. (6.1 ± 1.2 , 14.3 ± 1.2 , 12.4 ± 1.5 , 7.1 ± 0.9 , and 5.2 ± 0.3 % ID/g at 5, 24, 48, 72, and 96 h p.i. respectively; $n=4$; Fig. 4a, d).

Administering a blocking dose of TRC105 2 h before ^{89}Zr -Df-TRC105 injection reduced the tumor uptake to background level ($p < 0.01$ at all time points examined when compared with mice injected with ^{89}Zr -Df-TRC105 alone; Figs. 3a and 4b, d), which clearly indicated CD105 specificity of the tracer in vivo. On the other hand, liver uptake of ^{89}Zr -Df-TRC105 was significantly higher at all time points examined when a blocking dose of TRC105 was injected (31.4 ± 7.3 , 27.4 ± 3.8 , 25.6 ± 4.4 , 22.3 ± 7.1 , and 8.9 ± 1.9 % ID/g at 5, 24, 48, 72, and 96 h p.i. respectively; $n=4$). Radioactivity in the blood (2.2 ± 0.7 , 1.3 ± 0.4 , 0.9 ± 0.1 , 1.1 ± 0.3 , and 0.3 ± 0.1 % ID/g at 5, 24, 48, 72, and 96 h p.i. respectively; $n=4$) was also much lower in the “blocking” group (Fig. 4b). Together, these results suggest much faster hepatic clearance of the tracer when most CD105 in the mice was already bound by preinjected TRC105, thereby leaving no CD105 for ^{89}Zr -Df-TRC105 to bind to.

To further investigate the CD105 specificity of ^{89}Zr -Df-TRC105, ^{89}Zr -Df-cetuximab was used as an isotype-matched

Fig. 3 Small-animal PET imaging of 4T1 tumor-bearing mice. **a** Serial coronal PET images at 5, 24, 48, 72, and 96 h after injection of ^{89}Zr -Df-TRC105, 2 mg of TRC105 before ^{89}Zr -Df-TRC105 (i.e. blocking), or ^{89}Zr -Df-cetuximab. Tumors are indicated by *arrowheads*. **b** Representative PET/CT images of ^{89}Zr -Df-TRC105 in 4T1 tumor-bearing mice at 48 h p.i.



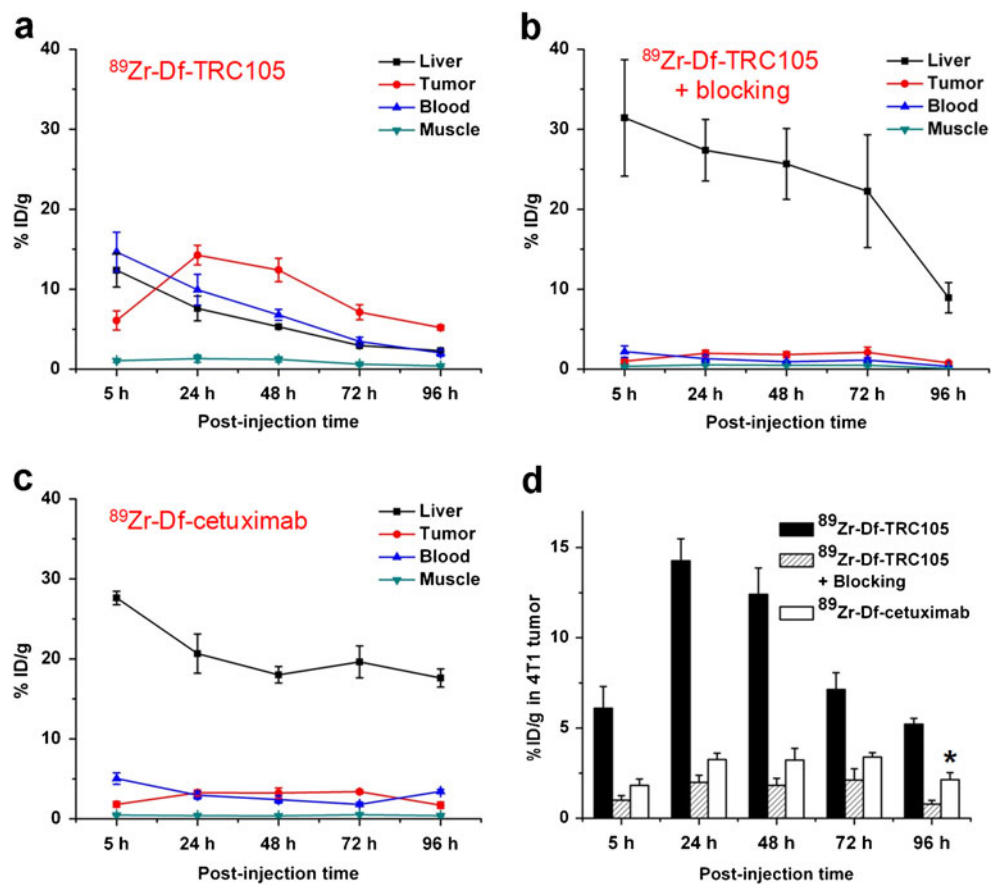
control. Both TRC105 and cetuximab are human/murine chimeric IgG1 mAbs. Since cetuximab does not cross-react with murine tissues, it serves as an excellent control for investigating tracer uptake in the tumor due to passive targeting only (i.e. the enhanced permeability and retention effect). As can be seen in Figs. 3a and 4c, d, the 4T1 tumor uptake of ^{89}Zr -Df-cetuximab was at the background level ($<3.5\% \text{ID/g}$) and significantly lower than that of ^{89}Zr -Df-TRC105 at all time points examined ($p < 0.01$ at 5, 24, 48, and 72 h p.i.; $p < 0.05$ at 96 h p.i.; $n = 4$), which again confirms the CD105 specificity of ^{89}Zr -Df-TRC105 in vivo.

Biodistribution studies

A group of four mice were injected with ^{89}Zr -Df-TRC105 and euthanized at 24 h p.i. for biodistribution studies (Fig. 5a). Besides the liver, the kidneys also had significant

tracer uptake at 24 h p.i., but the absolute uptake was significantly lower than that in the 4T1 tumor. Tracer uptake in all other tissues was also lower than in the tumor. All other mice were euthanized after the last PET scan at 96 h p.i. for biodistribution and immunofluorescence staining studies to validate the in vivo PET data. Comparing the biodistribution data at 24 h and 96 h p.i., ^{89}Zr -Df-TRC105 uptake in most tissues declined significantly over time, yet the tumor uptake remained prominent, which was indicative of specific interactions between an antibody and its antigen. Starting from 24 h p.i., 4T1 tumor uptake of the tracer was higher than that of all major organs in mice, thus providing excellent contrast with a tumor/muscle ratio of 24.8 ± 4.3 at 96 h p.i. ($n = 4$). Preinjection of a blocking dose of TRC105 led to a significant decrease in 4T1 tumor uptake and an increase in liver uptake of ^{89}Zr -Df-TRC105 ($p < 0.01$; $n = 4$; Fig. 5b), corroborating the PET findings.

Fig. 4 Quantitative ROI analysis of the PET data.
a Time–activity curves of the tumor, liver, blood, and muscle upon intravenous injection of ^{89}Zr -Df-TRC105 into 4T1 tumor-bearing mice ($n=4$).
b Time–activity curves of the tumor, liver, blood, and muscle upon intravenous injection of ^{89}Zr -Df-TRC105, after a blocking dose of TRC105, into 4T1 tumor-bearing mice ($n=4$).
c Time–activity curves of the tumor, liver, blood, and muscle upon intravenous injection of ^{89}Zr -Df-cetuximab into 4T1 tumor-bearing mice ($n=4$).
d Comparison of the 4T1 tumor uptake of ^{89}Zr -Df-TRC105, ^{89}Zr -Df-TRC105 after a blocking dose of TRC105, and ^{89}Zr -Df-cetuximab. All p values <0.01 when compared with ^{89}Zr -Df-TRC105, except $*p<0.05$



A comparison of the biodistribution data between the two tracers at 96 h p.i. revealed that the uptake of ^{89}Zr -Df-cetuximab was higher than or similar to that of ^{89}Zr -Df-TRC105 in most organs except the 4T1 tumor (Fig. 5c), which again indicated specific tumor targeting of ^{89}Zr -Df-TRC105. Overall, the quantification results obtained from biodistribution studies and PET scans matched very well, confirming that quantitative ROI analysis of non-invasive PET scans truly reflected the tracer distribution in vivo.

Histology

Immunofluorescence CD105/CD31 costaining of various tissues revealed that CD105 expression in the 4T1 tumor was primarily on the tumor vasculature, as evidenced by excellent colocalization of CD105 and CD31 staining and very weak signal on the 4T1 tumor cells (Fig. 6). Since CD105 is only expressed on actively proliferating endothelial cells, many of the mature vessels had significantly lower CD105 expression (indicated by arrowheads in Fig. 6) than in the neovasculature. The tumor vasculature is more actively proliferating in the peripheral region than in the center, therefore tumor uptake of the tracer is rather heterogeneous (i.e. higher uptake in the peripheral region and lower uptake in the tumor center).

CD105 staining of mouse liver and spleen both gave a very low signal, indicating that these tissues do not have significant levels of CD105 expression. Thus, uptake of ^{89}Zr -Df-TRC105 in liver/spleen was largely unrelated to CD105 binding and more likely related to nonspecific capture by the reticuloendothelial system and hepatic clearance of the tracer. A certain level of CD105 expression was observed in the kidney slices (mostly in the renal medulla) which likely caused appreciable renal uptake of ^{89}Zr -Df-TRC105, since full-length antibodies do not undergo renal clearance and because of the superb stability of ^{89}Zr -Df and Df-TRC105 there will be no significant amounts of ^{89}Zr -containing low-molecular weight species formed. Taken together, the ex vivo findings corroborated the in vivo results for ^{89}Zr -Df-TRC105, and thus further investigation and application of this tracer is warranted.

Discussion

Over the last decade, mounting preclinical and clinical data have suggested a promising future for ^{89}Zr -based immuno-PET in the management of cancer patients. The choice of Df as the chelator for ^{89}Zr is attractive because it has been safely used in the clinic for many years. In previous and

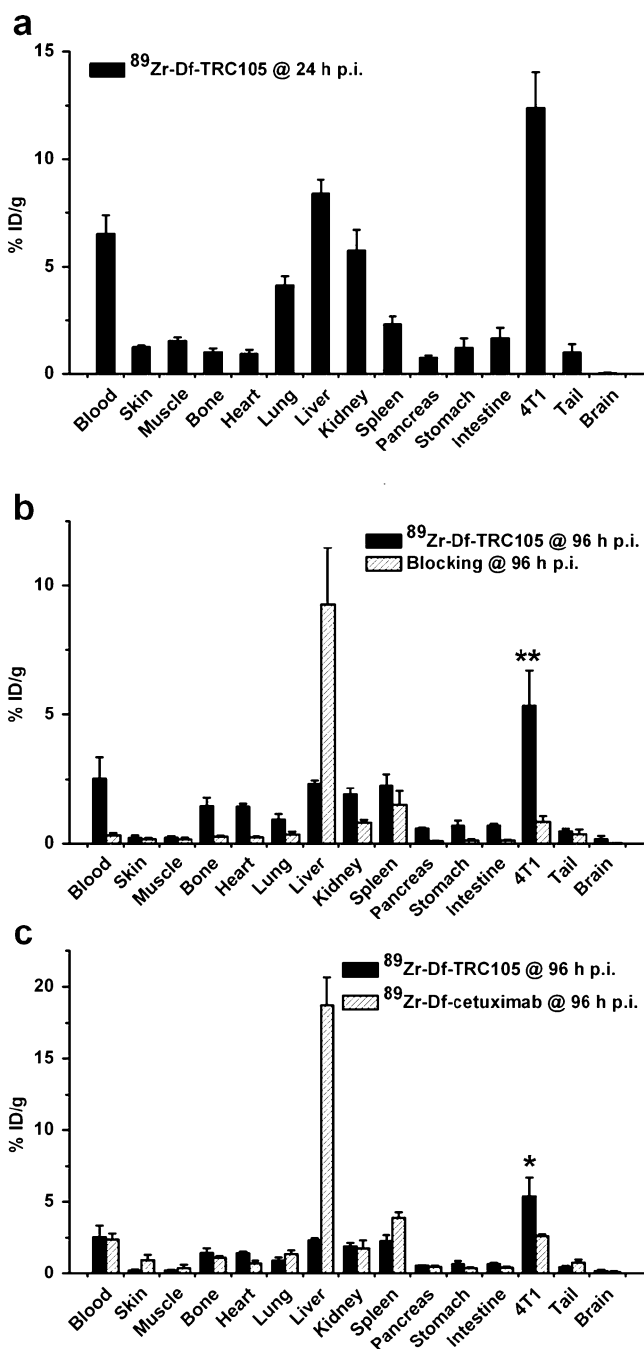


Fig. 5 Biodistribution studies in 4T1 tumor-bearing mice. **a** Biodistribution of ^{89}Zr -Df-TRC105 at 24 h p.i. ($n=4$). **b** Biodistribution of ^{89}Zr -Df-TRC105 and ^{89}Zr -Df-TRC105 after a blocking dose of TRC105 at 96 h p.i. ($n=4$). **c** Biodistribution of ^{89}Zr -Df-TRC105 and ^{89}Zr -Df-cetuximab at 96 h p.i. ($n=4$). * $p<0.05$, ** $p<0.01$

ongoing clinical studies, neither adverse reactions nor significant changes in blood and urine values have been observed after injection of Df-containing conjugates [2, 3]. In addition, no antibody responses directed against the Df chelate have been observed, indicating that its immunogenicity

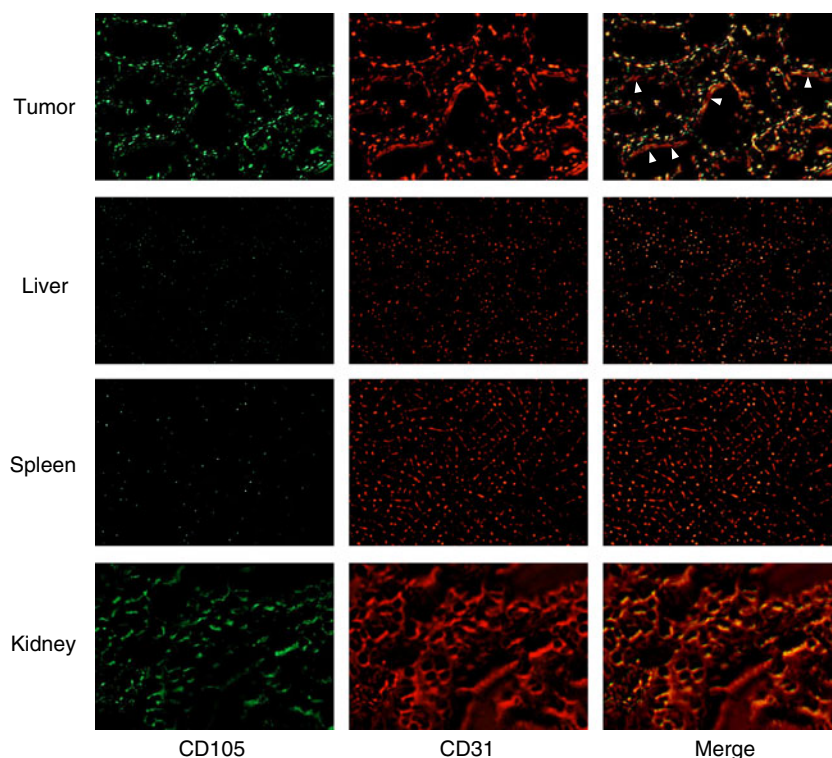
is very low [34]. With a new bifunctional chelator (i.e. Df-Bz-NCS) that recently became commercially available, it is expected that ^{89}Zr -based immunoPET will be the focus of more widespread future investigations.

The currently accepted standard method for quantifying angiogenesis is to assess microvessel density by performing CD105 immunohistochemistry on tumor tissue, an independent prognostic factor for survival in patients with many types of solid tumor [10, 11]. CD105 has the advantage of being selectively expressed on proliferating endothelial cells at significantly higher levels (up to 3×10^6 copies per cell) than other angiogenic targets such as the vascular endothelial growth factor receptors (less than 0.2×10^6 copies per cell) [30]. Noninvasive imaging of CD105 expression has the potential to accelerate antiangiogenic drug development by providing a reliable measure of angiogenesis in the entire body as an intact system, thereby facilitating individualized treatment monitoring and dose optimization in animal models, clinical trials, and ultimately in the day-to-day management of cancer patients. Therefore, the goal of this study was to develop a CD105-specific PET tracer. We have achieved this goal, and investigated TRC105 and its conjugates in vitro, in vivo, and ex vivo.

One key challenge in antibody labeling is to minimize the potential interference with its antigen binding affinity/specificity. There is only one lysine residue in each of the complementarity determining regions of TRC105 [11], which has a total of about 1,400 amino acid residues and about 70 lysines, and thus the possibility of Df conjugation at the lysine residue within the complementarity determining region is extremely low. Coupling of Df-Bz-NCS to mAbs was very efficient, and it has been reported that a reproducible chelate/mAb ratio of 1.5:1 can be obtained using only a three-fold molar excess of Df-Bz-NCS (which was adopted in this study) [27]. Such a low chelate/mAb ratio can adequately avoid alteration of the immunoreactivity (and pharmacokinetics) of TRC105, which was confirmed by FACS analysis and microscopy studies (Fig. 2).

The in vivo stability of radiometal-labeled antibodies is always a concern. To confirm that the tumor uptake of ^{89}Zr -Df-TRC105 visualized by noninvasive PET imaging was indeed CD105-specific, various control experiments (e.g. a blocking study and the use of an isotype-matched control) and in vitro/ex vivo experiments (e.g. FACS, microscopy, and histological studies) were performed for validation purposes. Based on the available literature data, the ^{89}Zr -Df conjugate is very stable in vivo [2, 33]. Therefore, the key to in vivo stability and antigen binding affinity of an ^{89}Zr -based tracer lies in the stability of the Df-antibody conjugate (Df-TRC105 in this case). To investigate this aspect, we incubated Df-TRC105 in complete mouse serum at 37°C for up to 7 days and observed no change in CD105

Fig. 6 Immunofluorescence CD105/CD31 double-staining of the 4T1 tumor, liver, spleen, and kidney tissue sections. TRC105 and AlexaFluor488-labeled goat anti-human IgG were used for CD105 staining (*green*). Afterwards, the tissue slices were stained with rat anti-mouse CD31 antibody and Cy3-labeled donkey anti-rat IgG (*red*). Note that CD105 expression is high on newly formed blood vessels but not on mature vessels, which exhibit predominantly CD31 staining (*arrowheads*). CD105 expression levels in the liver and spleen are much lower than in the tumor vessels. Significant levels of CD105 expression are also observed in the renal medulla. All images were acquired under the same conditions and are displayed at the same scale ($\times 200$)



binding affinity/specificity based on FACS analysis, which confirmed the superb stability of the tracer.

The rationale for choosing the 4T1 murine breast cancer model in this study is that the parent antibody of TRC105 (SN6j, a mAb of murine origin which binds to CD105) has been shown to be an effective antiangiogenic agent in this model [35]. Further, this is a rapidly growing tumor. Thus it has highly angiogenic tumor vasculature (Fig. 6) which is expected to provide sufficient target density for imaging applications. One limitation of this model is that the tumor vasculature is of murine origin. TRC105 has significantly higher affinity for human CD105 than for its murine homolog [36]. Thus, the 4T1 tumor model is not optimal for testing TRC105. When compared with other antibody-based PET tracers [31, 37, 38], tumor uptake in this study was relatively low (about 14 %ID/g at the peak). This is largely due to two facts. First, ^{89}Zr -Df-TRC105 targets the tumor vasculature but not the tumor cells. There are significantly fewer tumor vascular endothelial cells than tumor cells, which are the targets of most antibodies used for cancer imaging. Second, the affinity of TRC105 for murine endothelial cells is lower than its affinity for human endothelial cells.

For future investigation, the following strategies may be adopted to better mimic the clinical situation and further improve the tumor uptake/contrast: stably transfect 4T1 cells with human CD105, use transgenic mice with human tumor vasculature, or test an anti-CD105 antibody that binds with high affinity to murine CD105. Follow-up

studies are currently underway. In addition, studies have shown that tumor uptake of certain antibody-based PET tracers increases significantly with higher specific activity of the tracer [39]. Therefore, with further improvement in the specific activity of ^{89}Zr and optimization of the radiochemistry, tumor uptake of ^{89}Zr -Df-TRC105 in the currently used 4T1 model may be further improved in future studies. Nonetheless, excellent tumor contrast was achieved in this study, which justifies optimism that this tracer may perform better in cancer patients than in the murine models reported here.

One interesting finding from this study was the clear difference between blood clearance and biodistribution patterns of the two PET tracers, where the uptake of ^{89}Zr -Df-cetuximab in the liver was much higher and faster than that of ^{89}Zr -Df-TRC105 (Figs. 3 and 4). Many factors can affect the circulation half-life of an antibody, and antigen binding is only one of them. The neonatal Fc receptor (FcRn), which binds to the CH_2 - CH_3 hinge regions in the constant region (Fc) of IgG antibodies, plays a major role in their serum half-life [40]. Although TRC105 and cetuximab are isotype-matched chimeric antibodies, their amino acid sequences in the Fc region may be different [41]. In addition, variable glycosylation patterns in the Fc regions also add to variability, in addition to variability in amino acid sequences. Thus, the immunocompetent Balb/c mouse may recognize them with very different efficiency, which leads to different blood clearance rate and liver uptake.

In several other studies with ^{89}Zr -labeled antibodies, the tumor uptake reached a peak at around 24 h and remained stable for up to a week [33, 39]. Due to the fast-growing nature of the 4T1 tumor used in this study, although the total tumor uptake of ^{89}Zr -Df-TRC105 is quite steady over a period of 4 days, the %ID/g values did drop over time since the tumor volumes at 72 h and 96 h were $189\pm 34\%$ and $221\pm 25\%$ of their original volumes at the time of tracer injection ($n=4$). It has been reported that $^{89}\text{ZrCl}_4$ is mostly taken up by the liver and ^{89}Zr -Df undergoes renal excretion [33]. The low liver and kidney uptake of radioactivity observed in this study further confirms the superb stability of ^{89}Zr -Df-TRC105 in vivo. Regarding potential clinical translation, quantitative correlation of PET tracer uptake with the CD105 expression level would be highly desirable for treatment monitoring applications, as it would be ideal to noninvasively measure the changes of CD105 expression quantitatively, rather than qualitatively, in each individual patient upon antiangiogenic treatment.

Conclusion

We successfully investigated ^{89}Zr -labeled TRC105, a human–murine chimeric mAb recognizing both human and murine CD105, both in vitro and in vivo. Small-animal PET imaging revealed rapid, persistent, CD105-specific uptake of ^{89}Zr -Df-TRC105 in the 4T1 tumor, which was further validated by in vitro and ex vivo experiments. Since TRC105 is already under clinical investigation, and its therapeutic efficacy has been shown in various animal tumor models and certain cancer patients, this study identified a new avenue for tumor angiogenesis-related research and future clinical translation of ^{89}Zr -Df-TRC105 is warranted to investigate its use in the evaluation of the pharmacokinetics, tumor-targeting, dose optimization, and dose interval of TRC105 and TRC105-based cancer therapeutic agents in the clinic. In addition, ^{89}Zr -Df-TRC105 may also be useful in patient selection and monitoring of therapeutic response to various antiangiogenic therapies.

Acknowledgments This work was supported in part by the University of Wisconsin Carbone Cancer Center, the NIH through the UW Radiological Sciences Training Program 5 T32 CA009206-32, NCRR 1UL1RR025011, a DOD BCRP Postdoctoral Fellowship, and a DOD PCRP IDEA Award. The authors also thank Dr. Jason P. Holland and Dr. Jason S. Lewis for sharing their expertise on ^{89}Zr production and radiochemistry, Dr. Anna Wu and Dr. David M. Goldenberg for helpful discussions, Dr. Martin Shafer at the University of Wisconsin State Hygiene Laboratory for performing the ICPMS study, and Dr. Jamey P. Weichert and Mohammed Farhoud for their help with the PET scans.

Conflicts of interest B.R.L. is an employee of TRACON Pharmaceuticals, Inc. The other authors declare no conflicts of interest.

References

1. Wu AM. Antibodies and antimatter: the resurgence of immuno-PET. *J Nucl Med.* 2009;50:2–5.
2. van Dongen GA, Vosjan MJ. Immuno-positron emission tomography: shedding light on clinical antibody therapy. *Cancer Biother Radiopharm.* 2010;25:375–85.
3. Zhang Y, Hong H, Cai W. PET tracers based on zirconium-89. *Curr Radiopharm* 2011;4:131–9
4. Dijkers EC, Oude Munnink TH, Kosterink JG, Brouwers AH, Jager PL, de Jong JR, et al. Biodistribution of ^{89}Zr -trastuzumab and PET imaging of HER2-positive lesions in patients with metastatic breast cancer. *Clin Pharmacol Ther.* 2010;87:586–92.
5. Cai W, Chen X. Multimodality molecular imaging of tumor angiogenesis. *J Nucl Med.* 2008;49 Suppl 2:113S–28S.
6. Cai W, Chen X. Multimodality imaging of vascular endothelial growth factor and vascular endothelial growth factor receptor expression. *Front Biosci.* 2007;12:4267–79.
7. Cai W, Niu G, Chen X. Imaging of integrins as biomarkers for tumor angiogenesis. *Curr Pharm Des.* 2008;14:2943–73.
8. Dijkgraaf I, Boerman OC. Radionuclide imaging of tumor angiogenesis. *Cancer Biother Radiopharm.* 2009;24:637–47.
9. Dallas NA, Samuel S, Xia L, Fan F, Gray MJ, Lim SJ, et al. Endoglin (CD105): a marker of tumor vasculature and potential target for therapy. *Clin Cancer Res.* 2008;14:1931–7.
10. Fonsatti E, Nicolay HJ, Altomonte M, Cove A, Maio M. Targeting cancer vasculature via endoglin/CD105: a novel antibody-based diagnostic and therapeutic strategy in solid tumours. *Cardiovasc Res.* 2010;86:12–9.
11. Seon BK, Haba A, Matsuno F, Takahashi N, Tsujie M, She X, et al. Endoglin-targeted cancer therapy. *Curr Drug Deliv.* 2011;8:135–43.
12. Cai W, Rao J, Gambhir SS, Chen X. How molecular imaging is speeding up antiangiogenic drug development. *Mol Cancer Ther.* 2006;5:2624–33.
13. Zhang Y, Yang Y, Hong H, Cai W. Multimodality molecular imaging of CD105 (Endoglin) expression. *Int J Clin Exp Med.* 2011;4:32–42.
14. Zhang D, Feng XY, Henning TD, Wen L, Lu WY, Pan H, et al. MR imaging of tumor angiogenesis using sterically stabilized Gd-DTPA liposomes targeted to CD105. *Eur J Radiol.* 2009;70:180–9.
15. Bredow S, Lewin M, Hofmann B, Marecos E, Weissleder R. Imaging of tumour neovasculature by targeting the TGF-beta binding receptor endoglin. *Eur J Cancer.* 2000;36:675–81.
16. Costello B, Li C, Duff S, Butterworth D, Khan A, Perkins M, et al. Perfusion of ^{99m}Tc -labeled CD105 Mab into kidneys from patients with renal carcinoma suggests that CD105 is a promising vascular target. *Int J Cancer.* 2004;109:436–41.
17. Fonsatti E, Jekunen AP, Kairemo KJ, Coral S, Snellman M, Nicotra MR, et al. Endoglin is a suitable target for efficient imaging of solid tumors: in vivo evidence in a canine mammary carcinoma model. *Clin Cancer Res.* 2000;6:2037–43.
18. Korpanty G, Carbon JG, Grayburn PA, Fleming JB, Brekken RA. Monitoring response to anticancer therapy by targeting microbubbles to tumor vasculature. *Clin Cancer Res.* 2007;13:323–30.
19. Korpanty G, Grayburn PA, Shohet RV, Brekken RA. Targeting vascular endothelium with avidin microbubbles. *Ultrasound Med Biol.* 2005;31:1279–83.
20. Cui S, Lu SZ, Chen YD, He GX, Liu JP, Song ZY, et al. Relationship between intravascular ultrasound imaging features of coronary plaques and soluble CD105 level in patients with coronary heart disease. *Chin Med J Engl.* 2007;120:595–7.
21. Hong H, Yang Y, Zhang Y, Engle JW, Barnhart TE, Nickles RJ, et al. Positron emission tomography imaging of CD105 expression during tumor angiogenesis. *Eur J Nucl Med Mol Imaging.* 2011;38:1335–43.

22. Yang Y, Zhang Y, Hong H, Liu G, Leigh B, Cai W. In vivo near-infrared fluorescence imaging of CD105 expression during tumor angiogenesis. *Eur J Nucl Med Mol Imaging*. 2011. doi:10.1007/s00259-011-1886-x
23. Lee SY, Hong YD, Felipe PM, Pyun MS, Choi SJ. Radiolabeling of monoclonal anti-CD105 with ¹⁷⁷Lu for potential use in radioimmunotherapy. *Appl Radiat Isot*. 2009;67:1366–9.
24. Mendelson DS, Gordon MS, Rosen LS, Hurwitz H, Wong MK, Adams BJ, et al. Phase I study of TRC105 (anti-CD105 [endoglin] antibody) therapy in patients with advanced refractory cancer. *J Clin Oncol*. 2010;28:15s.
25. Meijs WE, Herscheid JDM, Haisma HJ, Pinedo HM. Evaluation of desferal as a bifunctional chelating agent for labeling antibodies with Zr-89. *Int J Rad Appl Instrum A*. 1992;43:1443–7.
26. Vosjan MJ, Perk LR, Visser GW, Budde M, Jurek P, Kiefer GE, et al. Conjugation and radiolabeling of monoclonal antibodies with zirconium-89 for PET imaging using the bifunctional chelate p-isothiocyanatobenzyl-desferrioxamine. *Nat Protoc*. 2010;5:739–43.
27. Perk LR, Vosjan MJ, Visser GW, Budde M, Jurek P, Kiefer GE, et al. p-Isothiocyanatobenzyl-desferrioxamine: a new bifunctional chelate for facile radiolabeling of monoclonal antibodies with zirconium-89 for immuno-PET imaging. *Eur J Nucl Med Mol Imaging*. 2010;37:250–9.
28. Wang H, Cai W, Chen K, Li ZB, Kashafi A, He L, et al. A new PET tracer specific for vascular endothelial growth factor receptor 2. *Eur J Nucl Med Mol Imaging*. 2007;34:2001–10.
29. Holland JP, Sheh Y, Lewis JS. Standardized methods for the production of high specific-activity zirconium-89. *Nucl Med Biol*. 2009;36:729–39.
30. Takahashi N, Haba A, Matsuno F, Seon BK. Antiangiogenic therapy of established tumors in human skin/severe combined immunodeficiency mouse chimeras by anti-endoglin (CD105) monoclonal antibodies, and synergy between anti-endoglin antibody and cyclophosphamide. *Cancer Res*. 2001;61:7846–54.
31. Cai W, Wu Y, Chen K, Cao Q, Tice DA, Chen X. In vitro and in vivo characterization of ⁶⁴Cu-labeled Abegrin, a humanized monoclonal antibody against integrin alpha v beta 3. *Cancer Res*. 2006;66:9673–81.
32. Cai W, Chen K, Mohamedali KA, Cao Q, Gambhir SS, Rosenblum MG, et al. PET of vascular endothelial growth factor receptor expression. *J Nucl Med*. 2006;47:2048–56.
33. Holland JP, Divilov V, Bander NH, Smith-Jones PM, Larson SM, Lewis JS. ⁸⁹Zr-DFO-J591 for immunoPET of prostate-specific membrane antigen expression in vivo. *J Nucl Med*. 2010;51:1293–300.
34. Borjesson PK, Jauw YW, Boellaard R, de Bree R, Comans EF, Roos JC, et al. Performance of immuno-positron emission tomography with zirconium-89-labeled chimeric monoclonal antibody U36 in the detection of lymph node metastases in head and neck cancer patients. *Clin Cancer Res*. 2006;12:2133–40.
35. Tsujie M, Uneda S, Tsai H, Seon BK. Effective anti-angiogenic therapy of established tumors in mice by naked anti-human endoglin (CD105) antibody: differences in growth rate and therapeutic response between tumors growing at different sites. *Int J Oncol*. 2006;29:1087–94.
36. Matsuno F, Haruta Y, Kondo M, Tsai H, Barcos M, Seon BK. Induction of lasting complete regression of preformed distinct solid tumors by targeting the tumor vasculature using two new anti-endoglin monoclonal antibodies. *Clin Cancer Res*. 1999;5:371–82.
37. Cai W, Ebrahimnejad A, Chen K, Cao Q, Li ZB, Tice DA, et al. Quantitative radioimmunoPET imaging of EphA2 in tumor-bearing mice. *Eur J Nucl Med Mol Imaging*. 2007;34:2024–36.
38. Cai W, Chen K, He L, Cao Q, Koong A, Chen X. Quantitative PET of EGFR expression in xenograft-bearing mice using ⁶⁴Cu-labeled cetuximab, a chimeric anti-EGFR monoclonal antibody. *Eur J Nucl Med Mol Imaging*. 2007;34:850–8.
39. Heskamp S, van Laarhoven HW, Molkenboer-Kueneen JD, Franssen GM, Versleijen-Jonkers YM, Oyen WJ, et al. ImmunoSPECT and immunoPET of IGF-1R expression with the radiolabeled antibody R1507 in a triple-negative breast cancer model. *J Nucl Med*. 2010;51:1565–72.
40. Roopenian DC, Akilesh S. FcRn: the neonatal Fc receptor comes of age. *Nat Rev Immunol*. 2007;7:715–25.
41. Jefferis R, Lefranc MP. Human immunoglobulin allotypes: possible implications for immunogenicity. *MAbs*. 2009;1:332–8.